國 立 交 通 大 學

電 機 與 控 制 工 程 學 系

碩 士 論 文

利用次通道降峰法以降低正交分頻多工系統的峰均比

PAPR Reduction for OFDM Systems Using Subchannel Peak Reduction

研 究 生： 吳 芳 儀

指 導 教 授： 林 源 倍 博士

中華民國九十七年八月

PAPR Reduction for OFDM Systems Using Subchannel Peak Reduction

Student : Fang-Yi Wu Advisor : Yuan-Pei Lin

Department of Electrical and Control Engineering
National Chiao Tung University

Abstract

Recently there has been great interest in the Orthogonal Frequency Division Multiplexing (OFDM) systems. However one disadvantage of OFDM systems is high peak-to-average power ratio (PAPR). In this thesis, we will propose a new method called Subchannel Peak Reduction (SPR). The symbols of a few selected subchannels are chosen to multiple a rotation individually so that PAPR is reduced. Transmission rate is slightly lower. However, no side information bit is needed. The optimal solution of the rotation can be found by exhaustive search (SPR-ES). We will propose an iterative approach method (SPR-IT) to find suboptimal rotating for the selected subchannels. SPR-IT can have lower complexity than SPR-ES. Simulation results shows SPR-ES and SPR-IT can efficiently reduce the peak value of the transmitted signal. The simulations will demonstrate that our method provide a nice tradeoff between bit rate and PAPR reduction.

Contents

List of Figures

List of Tables

Chapter 1

Introduction

Orthogonal frequency division multiplexing (OFDM) [1] is a multicarrier modulation technique that has been used for many applications, such as wireless local area networks (WLANs) [2], digital video broadcasting (DVB) [3], and digital audio broadcasting (DAB) [4]. International standards making use of OFDM for high speed wireless communications are already established or being established by IEEE 802.11, IEEE 802.16, IEEE 802.20, and European Telecommunications Standards Institute (ETST) Broadcast Radio Access Network (BRAN) committees.

In OFDM systems, the input bit stream is coded as modulation symbols, e.g., quadrature amplitude modulation (QAM). The channel is divided into subchannels, each with a different frequency band. Modulation symbols of different subchannels carry the same number of bits because there is usually no bit/ power allocation in OFDM systems. The transmitter and receiver performance inverse Discrete Fourior Transform (IDFT) and Discrete Fourior Transform (DFT) computations respectively. At the transmitter, for each block, a certain redundancy known as cyclic prefix (CP) [5] is added. When the channel order is not large than the prefix length, inter block interference (IBI) can be easily removed by discarding the prefix at the receiver. The OFDM system is attractive because of its high-bit-rate transmission. However, an OFDM signal may have high peak to average power ratio (PAPR) at the transmitter which causes the power amplifier of the transmitter to operate in a low efficiency region [6]. How to reduce the

PAPR is an important issue in the design of transmitters.

Many schemes have been proposed to reduce the PAPR. One method is called clipping [7], which limits the peak envelope of the input signal to a desired maximum value. The clipping process is nonlinear and may causes in-band distortion and out-of-band radiation. Coding method in [8]-[10] are proposed to reduce PAPR by selecting some codewords with lower PAPR for transmission. Such coding techniques require large lookup tables for encoding and decoding. Therefore, it is fit for systems with a small number of subcarriers. The selective mapping (SLM) [11][12] and partial transmit sequence (PTS) [13] can efficiently lower the peak power of the OFDM transmitted signal. In the SLM approach, after multiplying some phase sequences to the input signal to generate different candidate signals, we can choose the one with the least PAPR to transmit. In the PTS method, the input sequence is divided into disjoint subblocks. Optimally combining those disjoint subblocks and phase factors can have a lower PAPR sequence. Both SLM and PTS need to send side information to express how the signal was produced. In the OFDM systems, blocks are grouped and sent in packets. The side information for PAPR reduction is transmitted as part of the preamble. The transmitter needs to generate all the blocks before the side information for PAPR is determined and encoded in the preamble. This leads to a higher complexity for the transmitter. If the decoder makes error then the receiver will not know how the transmitted signal is related to the original signal before using PAPR reduction method. Besides, the processes of SLM and PTS increase the computational complexity. The SLM method needs m M-point IDFT to generate m candidates. The PTS scheme needs $(\log_4 m + 1)$ M-point IDFT to generate m candidates when the rotation factors are chosen from $\{\pm 1, \pm j\}$. [14]-[16] are proposed at the cost of a minus performance degradation. Tone injection can reduce PAPR by increasing the constellation size. Then the points in the original constellation can be mapped into several equivalent points. The expanded constellation needs more transmission power.

In this thesis, we consider the problem of reducing PAPR with low computational complexity. We call the new method Subchannel Peak Reduction (SPR).

We choose a few subchannels as peak reduction (PR) subchannels. The symbols of the PR subchannels are chosen for the purpose of the PAPR reduction. The symbols of the PR subchannels may be rotated by multiplies of 180° or multiplies of 90° individually. For 180°-rotation case, if b bit constellation are used for all subchannels, on the PR subchannel there are $(b-1)$ bits can be transmitted. Bits are coded to symbol as usual on the non PR subchannel. For the decoder, the received symbol and its rotated by multiplies of 180° symbol are mapped to the same bits. In SPR method, by exhausting all possible combinations of rotations for the PR subchannel we can found the smallest PAPR. The solution is optimal and it is exhaustive search of the SPR method. We call it SPR-ES. The complexity can be reduced using a suboptimal rotation of the PR subchannel. It can be done by iterating PR subchannels one by one. The scheme is called SPR-IT and the PAPR performance is close to that of SPR-ES. SPR will decrease the transmission rate slightly. SPR provide a tradeoff between bit rate and PAPR reduction. However, no side information bit is needed.

1.1 Outline

- Chapter 2: The basic structure of OFDM systems and the PAPR of OFDM systems are presented. The common performance measure for PAPR reduction techniques will also be mentioned.

- Chapter 3: We will introduce two cases of tone injection method which was proposed by J. Tellado [6]. One used on real multicarrier systems and the other is for passband communication.

- Chapter 4: New method called Subchannel Peak Reduction will be proposed in this chapter. In section 4.1, we will see Exhaustive Search method. Iterative Approach scheme will be discused in section 4.2.

- Chapter 5: The calculations of complexity for Exhaustive Search, Iterative Approach, and tone injection for passband communication are in chapter5.

- Chapter 6: Some computer simulation results about PAPR and BER will be seen and the computational complexity comparison are also put in this chapter.
- Chapter 7: Conclusion is given in chapter 7.

1.2 Notations

1. **Bold faced** upper-case letters are used to represent matrices and **bold faced** lower-case letters are used to represent vectors.
2. $\mathbf{A}^{\dagger}$ denotes transpose-conjugate of $\mathbf{A}$.
3. $\mathbf{A}^{T}$ denotes transpose of $\mathbf{A}$.
4. The function $\mathrm{E}[x]$ denotes the average value or expect value of x.
5. The element-wise multiplication of a $M \times 1$ vector $\mathbf{g}$ and a $M \times 1$ vector $\mathbf{f}$ is a $M \times 1$ vector given by:

$$\mathbf{g} \,.\times \mathbf{f} = \begin{bmatrix} g_0 f_0 \\ g_1 f_1 \\ \vdots \\ g_{M-1} f_{M-1} \end{bmatrix}_{M \times 1} .$$

6. The notation $\mathbf{W}_M$ is used to represent the normalized $M \times M$ DFT matrix given by

$$[\mathbf{W}_M]_{kn} = \frac{1}{\sqrt{M}} e^{-j\frac{2\pi}{M}kn},$$

where $0 \leq k, n \leq M-1$.

Chapter 2

OFDM systems

2.1 The OFDM systems model

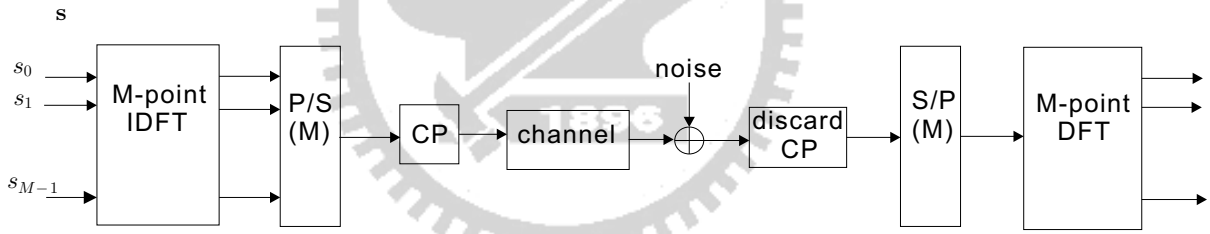

Figure 2.1: The OFDM system.

Fig. 2.1 is the block diagram of the OFDM system. The input symbol block $\mathbf{s}$ is a $M \times 1$ vector, $\mathbf{s} = [s_0, s_1, \cdots, s_{M-1}]^T$, where M is the number of subchannels. The element s_k in $\mathbf{s}$ represents the modulation symbol of the k-th subcarrier. The input symbol block passes through the M-point IDFT and the parallel to serial conversion (P/S) gets serial sample train. For every block of M data samples, the transmitter adds a cyclic prefix (CP) of length ν samples of the transmitted blocks. After CP process, the transmitted block of $M + \nu$ samples pass through the channel plus noise. With a proper insertion of CP, an FIR channel can be decomposed into M parallel AGN subchannels with a gain that depends on the channel. The efficiency of the transceiver is $\frac{M}{M+\nu}$, the larger the channel order is,

the larger the cyclic prefix is needed to eliminate ISI, and the lower the efficiency is. When the channel is additive white Gaussian noise (AWGN) channel, there is no inter symbol interference (ISI) and the transmission error comes from the channel noise only. At the receiver, after discarding the cyclic prefix called discard CP and serial to parallel (S/P) conversion gets the parallel samples. The DFT matrix is applied to the received parallel samples

In this thesis, we assume the channel order is not large than the prefix length ν so there is no IBI. For transmission, We can only consider an input block and an output block, ie., one-shot transmission.

2.2 The PAPR of OFDM systems

Although the OFDM system process has been discussed in section 2.1, we will see more of the transmitter part. We redraw the transmitter of the OFDM system in Fig. 2.2 and also add a symbol mapping block in front of the input symbol block $\mathbf{s}$.

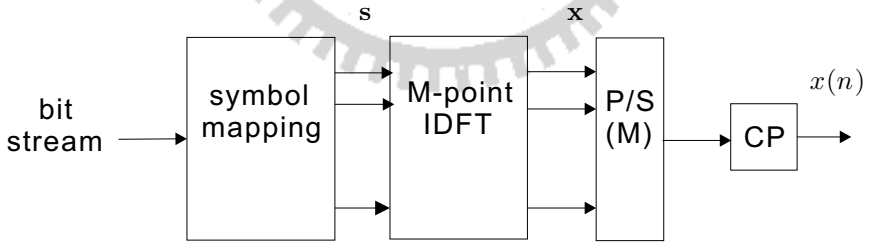

Figure 2.2: The transmitter of OFDM systems.

The bit stream consists of $0'$s and $1'$s. The symbol mapping block takes several bits of the bit stream and maps these bits to a real or complex symbol. The sequence $\mathbf{x}$ is generated by $\mathbf{s}$ and a normalized $M \times M$ IDFT matrix $\mathbf{W}^{\dagger}$,

$$\mathbf{x} = \mathbf{W}^{\dagger}\mathbf{s}, \tag{2.1}$$

where

$$\mathbf{W}^{\dagger} = \frac{1}{\sqrt{M}} \begin{pmatrix} 1 & 1 & \dots & 1 \\ 1 & W & \dots & W^{M-1} \\ \vdots & \vdots & \ddots & \vdots \\ 1 & W^{M-1} & \dots & W^{(M-1)^2} \end{pmatrix}^{\dagger},$$

and $W = e^{-j\frac{2\pi}{M}}$. The m-th subcarrier in $\mathbf{x}$ can be expressed as

$$x_m = \frac{1}{\sqrt{M}} \sum_{k=0}^{M-1} s_k e^{j2\pi km/M}, \quad 0 \le m \le M-1. \tag{2.2}$$

In Fig. 2.2, $x(n)$ is the transmitter output signal which is obtained by $\mathbf{x}$ passing through parallel to serial conversion and cyclic prefix operation. The PAPR of OFDM signal $x(n)$ is defined as

$$\text{PAPR} = \frac{\max_n \mid x(n) \mid^2}{\text{E}[\mid x(n) \mid^2]}, \tag{2.3}$$

where E[·] denotes the expectation operator. The parallel to serial conversion is to convert a set of parallel input data $\mathbf{x}$ to a serial stream. The cyclic prefix is to copy the last fewer samples at the end of each block and place them at the beginning. Both operations do not change the maximum value of $\mathbf{x}$, so the peak power do not change after these two processes. When the symbol mapping is decided, the average power is fixed. From above, we can find that $x(n)$ has the same peak power and the same average power as the IDFT output vector $\mathbf{x}$, therefore we can consider PAPR as the following equation instead,

$$\text{PAPR} = \frac{\max_m \mid x_m \mid^2}{\text{E}[\mid x_m \mid^2]}. \tag{2.4}$$

The cumulative distribution function (CDF) of the PAPR is one of the most frequently used performance measure for PAPR reduction techniques. In this thesis, the complementary cumulative distribution function (CCDF) is used instead of the CDF. The CCDF of the PAPR denotes the probability that the PAPR of a data block exceeds a given threshold (PAPR_0). CCDF is defined as:

$$\text{CCDF}(\text{PAPR}_0) = Prob(\text{PAPR} > \text{PAPR}_0). \tag{2.5}$$

The horizontal and vertical axes represent the threshold for the PAPR and the probability that the PAPR of a data block exceeds the threshold respectively. In Fig. 2.3, for PAPR thresholds, if a curve $a1$ has smaller horizontal values than the other curve $a2$, $a1$ has better PAPR performance than $a2$. From this phenomenon, the closer the CCDF is to the vertical axis, the better its PAPR characteristic is.

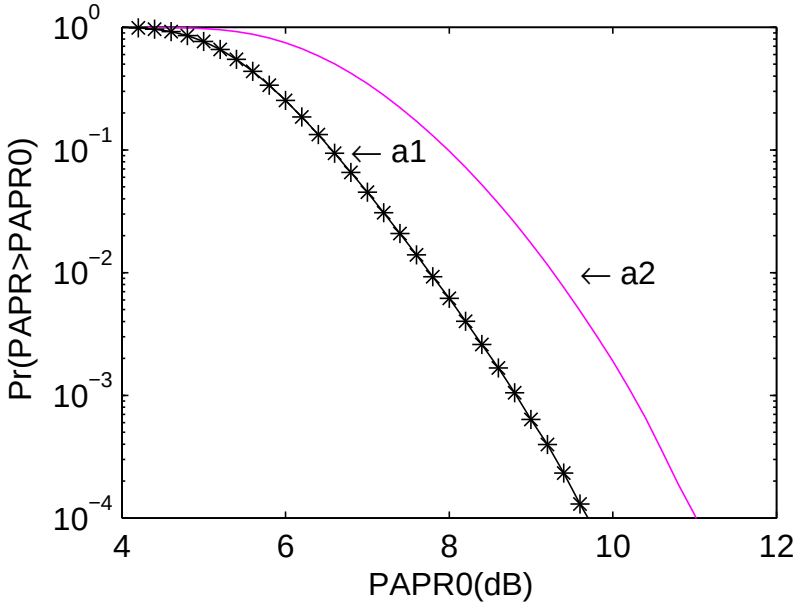

Figure 2.3: An example figure. a1 has better PAPR performance than a2.

Chapter 3

PAPR Reduction By Tone Injection [6]

In this chapter, we will briefly introduce the tone injection method which was proposed by J. Tellado [6]. In section 3.1, the usage of tone injection method for Real Multicarrier systems will be discussed. We will see this method using for passband communications in section 3.2.

3.1 Tone Injection for Real Multicarrier Systems

The basic idea of tone injection method is to let each of the point in the original basic constellation to map into several equivalent points in the expanded constellation. The above demand can be done by increasing the constellation size and it is equivalent to injecting a tone of the appropriate frequency and phase in the multicarrier symbol.

Assume a 2^b QAM (b-bit QAM) is used as a modulation scheme and the minimum distance between constellation points is d. Let s_k be the k-th modulation symbol of the input block obtained by mapping b bits to the 2^b QAM constellation. The real part of s_k is R_k and the imaginary part is I_k. Both R_k and I_k can take values from $\{\pm d/2, \pm 3d/2, \cdots, \pm(\sqrt{2^b}-1)d/2\}$. Now consider 16 QAM here and assume Gray codes are used as Fig. 3.1.

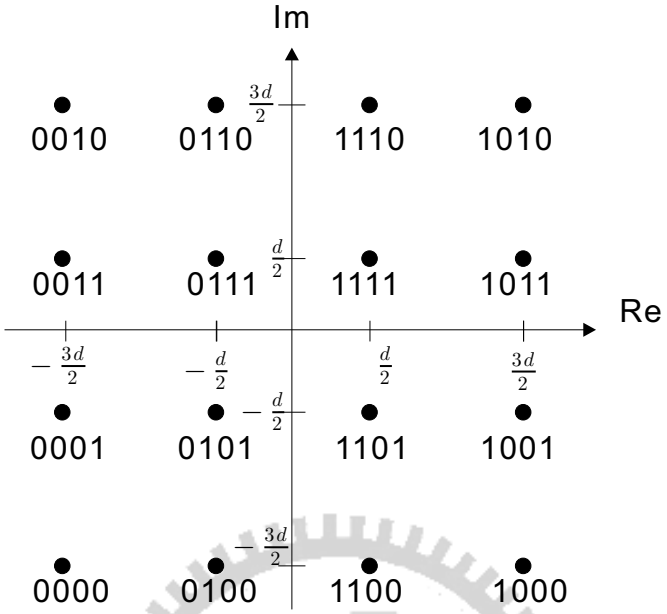

Figure 3.1: 16 QAM constellation and its Gray code mapping.

We take an example of $s_k = d/2 + j3d/2$ which is denoted by A in Fig. 3.2. We can see by subtracting or adding a fixed constant D to the real and imaginary part of s_k can enlarge the constellation, where $D = a \cdot d\sqrt{2^b}$ and a is a constant which is selected as $a \geq 1$. D is a real constant known by the transmitter and receiver. The original s_k can become

$$\bar{s_k} = s_k + p_k D + jq_k D \tag{3.1}$$

$$= (R_k + p_k D) + j(I_k + q_k D), \tag{3.2}$$

where p_k and q_k are integers and they can take values from $\{+1, -1, 0\}$. After picking p_k and q_k, point A can expand to another 8 points: $A1$ to $A8$. Every point on the original 16 QAM constellation can be expanded to another 8 points like the above example. If D is chosen in the special case where $a = 1$, and D is $d\sqrt{2^b}$, then the expanded constellation becomes a lattice (equally spaced points) [Kschischang et al., 1998a, Kschischang et al., 1998b,]. The expanded constellation is equivalent to a 9×16 QAM constellation which is in Fig. 3.3.

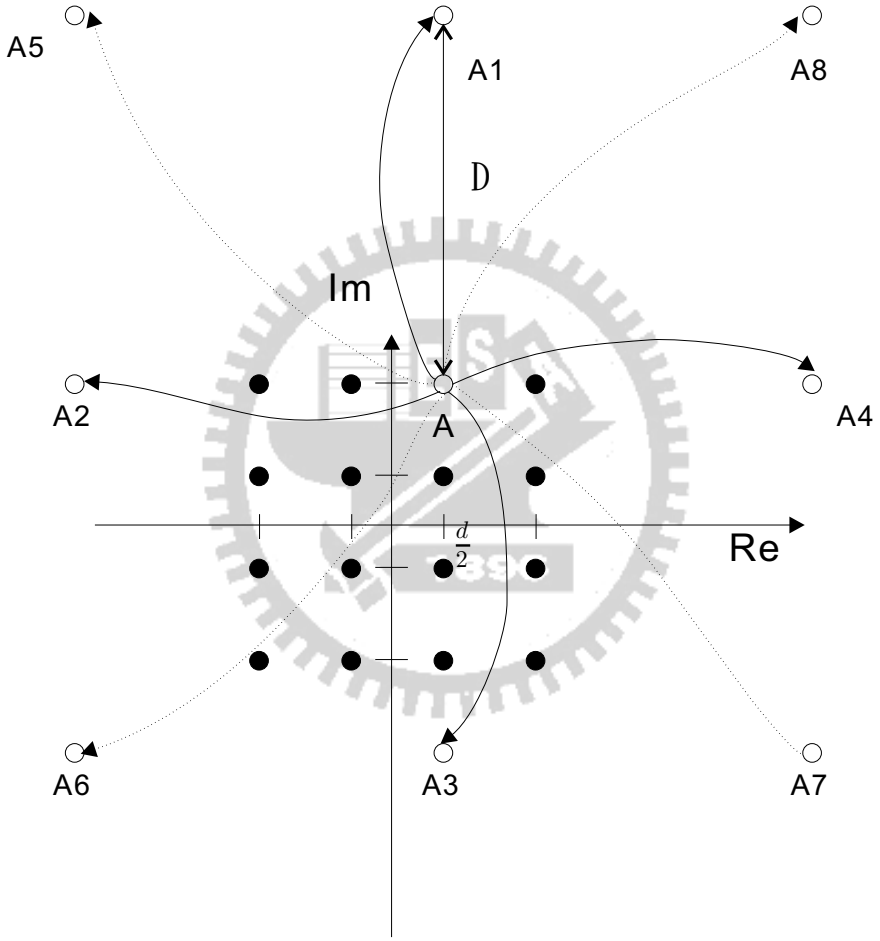

Figure 3.2: A example of a point A mapped to another 8 points.

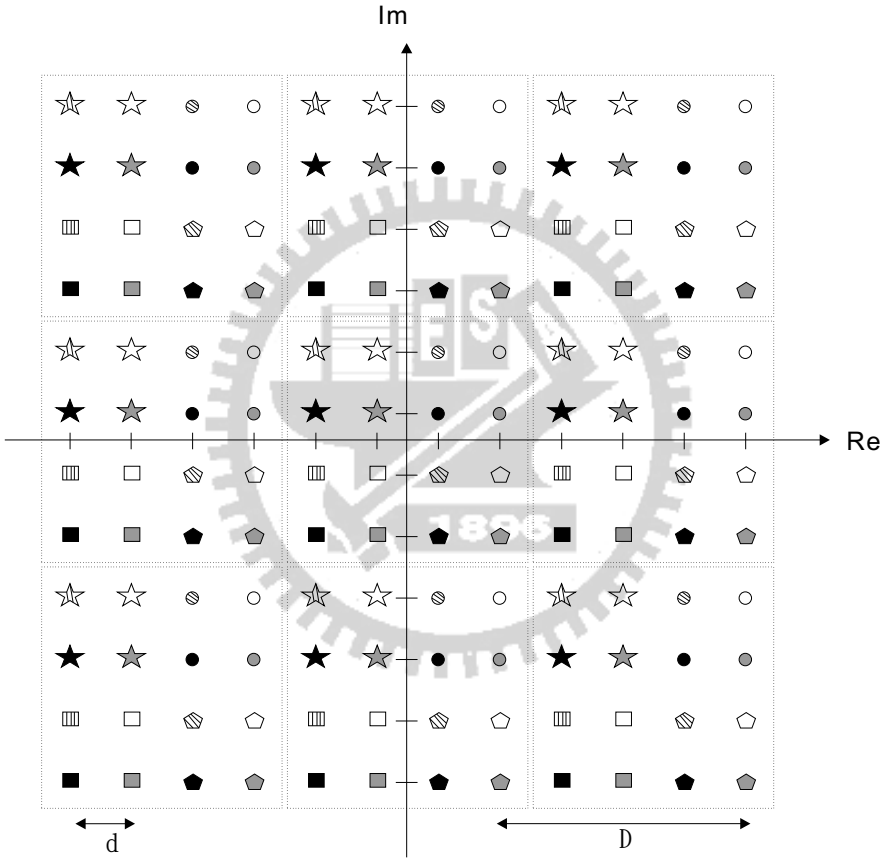

Figure 3.3: 9×16 QAM constellation.

In order to generate the real transmitted signals, the number of IDFT must be even and the input symbol block $\mathbf{s}$ has to be conjugate symmetric,

$$s_k = \begin{cases} s^*_{M-k}, & \text{otherwise} \\ 0, & \text{k} = 0, \frac{M}{2}. \end{cases} \tag{3.3}$$

The element of transmitted IDFT output $\mathbf{x}$ can be written as

$$x_n = \frac{1}{\sqrt{M}} \sum_{k=0}^{M-1} s_k e^{j2\pi kn/M}, \quad 0 \le n \le M-1 \tag{3.4}$$

$$= \frac{2}{\sqrt{M}} \sum_{k=0}^{\frac{M}{2}-1} s_k e^{j2\pi kn/M}. \tag{3.5}$$

Let $s_k = R_k + jI_k$,

$$x_n = \frac{2}{\sqrt{M}} \sum_{k=0}^{\frac{M}{2}-1} (R_k + jI_k) e^{j2\pi kn/M} \tag{3.6}$$

$$= \frac{2}{\sqrt{M}} \sum_{k=0}^{\frac{M}{2}-1} [R_k \cos(\frac{2\pi kn}{M}) - I_k \sin(\frac{2\pi kn}{M})]. \tag{3.7}$$

Using tone injection process is equivalent to adding a $M \times 1$ vector $\mathbf{c}$ to $\mathbf{s}$, where $c_k = p_k D + jq_k D$. This means that the input block $\mathbf{s}$ becomes $\mathbf{s} + \mathbf{c}$ which is in Fig. 3.4. IDFT is applied and the output is $\mathbf{x}$. x_n is the n-th subchannel of $\mathbf{x}$ and can be formulated as

$$x_n = \frac{1}{\sqrt{M}} \sum_{k=0}^{M-1} \bar{s_k} e^{j2\pi kn/M} \tag{3.8}$$

$$= \frac{1}{\sqrt{M}} \sum_{k=0}^{M-1} (s_k + c_k) e^{j2\pi kn/M}, \quad 0 \le n \le M-1. \tag{3.9}$$

Because D is known at the receiver, c_k can be removed at the receiver by applying a modulo-D on the real and imaginary part at the output of the DFT operator.

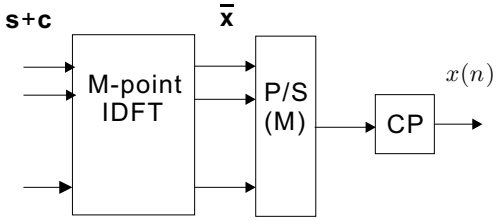

Figure 3.4: The transmitter plus tone injection method of the OFDM system.

For a real multicarrier system, assume x_{n_0} has the maximum value and $x_{n_0} > 0$. We can modify the n_0-th subchannel by tone injection method per dimension. It means that the real or imaginary part can be changed. Here we used tone injection scheme on the real dimension. Assume $\cos(\frac{2\pi k_0 n_0}{M}) = l$, $l > 0$ for a frequency k_0. The real part of k_0-th subchannel is going to be modified.

$$\begin{aligned} x_{n_0} &= \tfrac{2}{\sqrt{M}} \textstyle\sum_{k=0}^{\frac{M}{2}-1} [R_k \cos(\tfrac{2\pi k n_0}{M}) - I_k \sin(\tfrac{2\pi k n_0}{M})] \\ &= \tfrac{2}{\sqrt{M}} \textstyle\sum_{k=0, k\neq k_0}^{\frac{M}{2}-1} [R_k \cos(\tfrac{2\pi k n_0}{M}) - I_k \sin(\tfrac{2\pi k n_0}{M})] \\ &+ \tfrac{2}{\sqrt{M}} [R_{k_0} \cos(\tfrac{2\pi k_0 n_0}{M}) - I_{k_0} \sin(\tfrac{2\pi k_0 n_0}{M})]. \end{aligned} \tag{3.10}$$

We subtract R_{k_0} by D, x_{n_0} becomes $\bar{x}_{n_0}$:

$$\begin{aligned} \bar{x}_{n_0} &= \tfrac{2}{\sqrt{M}} \textstyle\sum_{k=0, k\neq k_0}^{\frac{M}{2}-1} [R_k \cos(\tfrac{2\pi k n_0}{M}) - I_k \sin(\tfrac{2\pi k n_0}{M})] \\ &+ \tfrac{2}{\sqrt{M}} [(R_{k_0} - D) \cos(\tfrac{2\pi k_0 n_0}{M}) - I_{k_0} \sin(\tfrac{2\pi k_0 n_0}{M})] \\ &= x_{n_0} - \tfrac{2}{\sqrt{M}} D \cos(\tfrac{2\pi k_0 n_0}{M}). \end{aligned} \tag{3.11}$$

We can see that in (3.11) $x_{n_0} > 0$ also both D and $\cos(\frac{2\pi k_0 n_0}{M})$ are positive, so $\bar{x}_{n_0}$ is smaller than x_{n_0}. This is meant that the peak reduction is $\frac{2}{\sqrt{M}} D \cos(\frac{2\pi k_0 n_0}{M})$. A similar argument follows for other permutations, for example when $\cos(\frac{2\pi k_0 n_0}{M}) < 0$, we can add D to R_{k_0} in order to lower $\bar{x}_{n_0}$. These ideas can also extend to $\sin(\frac{2\pi k n_0}{M})$ term easily. $\{a, b\}$ defined as the choice is a or b. There are 4 options

for each subchannel k_0. The general equation can be expressed as following,

$$\bar{x}_n = x_n + \frac{2}{\sqrt{M}}(\pm D)\{\cos, \sin\}(\frac{2\pi k_0 n}{M}), \quad n = 0, 1, \cdots, M-1. \quad (3.12)$$

3.2 Tone Injection for passband communications

The tone injection method for real multicarrier systems proposed by J. Tellado [6] was introduced in Section 3.1. For passband communication, we now extend this method to complex case.

For passband communication systems, because the values of IDFT output are complex, there is no restriction on the input symbols. Complex values can not compare with zero. Therefore, every input modulation symbol for each block needs to modify. The modification is the same as that section 3.1: expand the original 16 QAM constellation to a 9×16 QAM by adding or subtracting a constant D to the real and imaginary part of the subchannel, where D is $d\sqrt{2^b}$. After all the subchannels doing all the same modifications, find the sequence with the smallest PAPR. D is decided at first and both the transmitter and the receiver know the value. Using a modulo-D process can map the received signals back to the original constellation. Therefore, there is no bit lost to transform side information from the transmitter to the receiver. The expanded constellation will cause bigger transmission power. This will be discussed in the next paragraph.

We mark the horizontal and vertical axes as Fig. 3.5. Assume the all constellation points are equiprobable. The average energy ε_s of modulation symbols can be written as

$$\begin{aligned}
\varepsilon_s &= \frac{4}{16}[\sum_{k=1}^{4} {R_k}^2 + \sum_{k=1}^{4} {I_k}^2] && (3.13)\\
&= \frac{4}{16}[{R_1}^2 + {R_2}^2 + {R_3}^2 + {R_4}^2 + {I_1}^2 + {I_2}^2 + {I_3}^2 + {I_4}^2] && (3.14)\\
&= 2 \times \frac{4}{16}[(\frac{-3d}{2})^2 + (\frac{-d}{2})^2 + (\frac{d}{2})^2 + (\frac{3d}{2})^2] && (3.15)\\
&= \frac{10}{4}d^2. && (3.16)
\end{aligned}$$

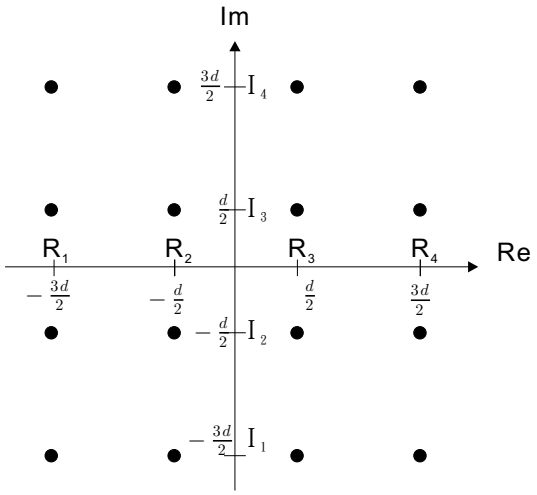

Figure 3.5: The marked horizontal and vertical axes of 16QAM.

The expanded 16 QAM constellation can be divided into three groups in Fig. 3.6. One is the original 16 QAM constellation in the middle. In part A both real and imaginary parts can be added or subtracted a constant D. Only one dimension is changed in part B. The signal power in part B is given by:

$$\begin{aligned}
\varepsilon_{s-B} &= \frac{4}{16}[\sum_{k=1}^{4}(R_k + D)^2 + \sum_{k=1}^{4} {I_k}^2] && (3.17)\\
&= \frac{4}{16}[\sum_{k=1}^{4}({R_k}^2 + 2R_kD + D^2) + \sum_{k=1}^{4} {I_k}^2] && (3.18)\\
&= \frac{4}{16}[\sum_{k=1}^{4}({R_k}^2 + {I_k}^2) + 4D^2 + 2(R_1D + R_2D + R_3D + R_4D)] && (3.19)\\
&= \frac{4}{16}[\sum_{k=1}^{4}({R_k}^2 + {I_k}^2)] + D^2 && (3.20)\\
&= \varepsilon_s + D^2. && (3.21)
\end{aligned}$$

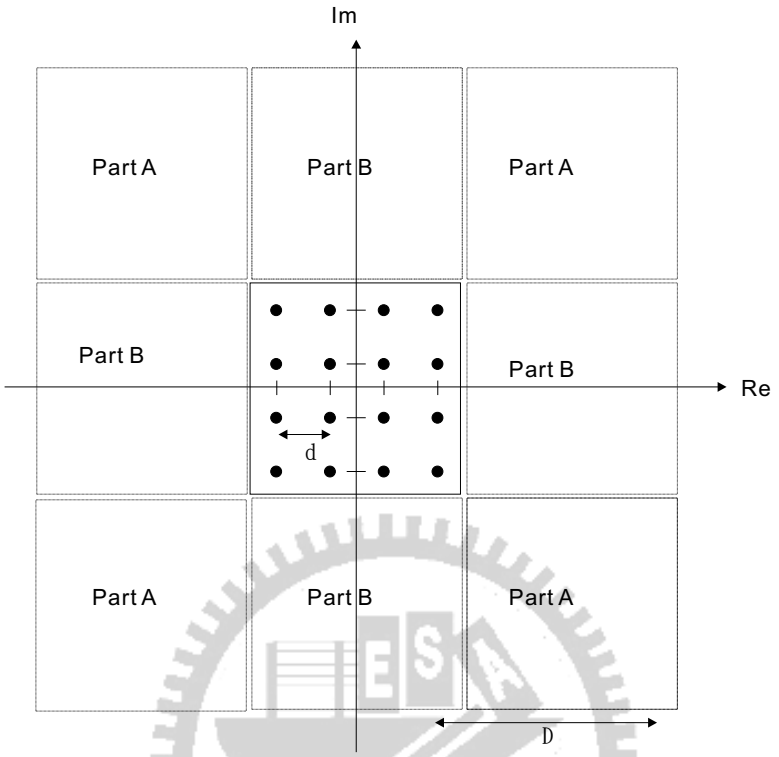

Figure 3.6: The expanded 16 QAM constellation can be divided into three groups, original 16 QAM, part A, and part B.

The signal power in part A is given by:

$$\begin{aligned}
\varepsilon_{s-A} &= \tfrac{4}{16}[\textstyle\sum_{k=1}^{4}(R_k + D)^2 + \sum_{k=1}^{4}(I_k + D)^2] \\
&= \tfrac{4}{16}[\textstyle\sum_{k=1}^{4}({R_k}^2 + {I_k}^2) + 8D^2 + 2(R_1 D + R_2 D \\
&+ R_3 D + R_4 D) + 2(I_1 D + I_2 D + I_3 D + I_4 D)] \qquad (3.22) \\
&= \tfrac{4}{16}[\textstyle\sum_{k=1}^{4}({R_k}^2 + {I_k}^2)] + 2D^2 \\
&= \varepsilon_s + 2D^2.
\end{aligned}$$

After expanding the constellation size, the signal power over this constellation

is ε_{s-new} becomes

$$\begin{aligned} \varepsilon_{s-new} &= \frac{1}{9}\varepsilon_s + \frac{4}{9}\varepsilon_{s-B} + \frac{4}{9}\varepsilon_{s-A} && (3.23) \\ &= \frac{1}{9}\varepsilon_s + \frac{4}{9}(\varepsilon_s + D^2) + \frac{4}{9}(\varepsilon_s + 2D^2) && (3.24) \\ &= \varepsilon_s + \frac{4}{3}D^2. && (3.25) \end{aligned}$$

Because only one subchannel is modified a at time, the signal power of every subchannel becomes

$$\begin{aligned} \varepsilon_{s'} &= \frac{63}{64}\varepsilon_s + \frac{1}{64}\varepsilon_{s-new} && (3.26) \\ &= \varepsilon_s + \frac{D^2}{48}. && (3.27) \end{aligned}$$

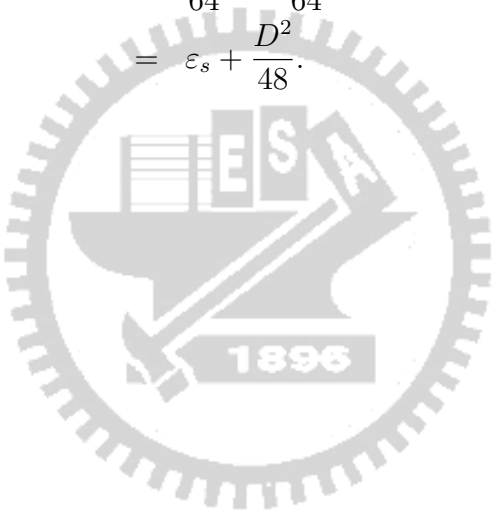

Chapter 4

The Subchannel Peak Reduction Method

In this chapter, we present a subchannel based PAPR reduction method that we called Subchannel Peak Reduction method. We choose a few subchannels, called peak reduction (PR) subchannels. The symbols of the PR subchannels are transmitting at a slightly lower rate so that PAPR is reduced. In particular, the symbols transmitted on the PR subchannels may be individually rotated by multiples of 180° to minimize PAPR. Fig. 4.1 shows an example of bits-to-symbol mapping for PR subchannels when the constellation is 16 QAM. The example given in Fig. 4.1(a) is for the case when the symbols on the PR subchannels may be rotated by multiples of 180° and Fig. 4.1(b) is for the case when the symbol can be rotated by multiples of 90°. In the following discussions, we will consider the case of 180° rotation first. The method can be extended to the 90°-rotation case latter. In other words, the same input bits may be mapped to s_k or $-s_k$, depending on which yields a smaller PAPR. If b-bit constellation are used for all subchannels, only $(b-1)$ bits can be transmitted on the PR subchannel. For non PR subchannels, bits are coded as symbol in the usual manner. Suppose the receiver output is $\hat{s}_k$ (before symbol detection). Then $\hat{s}_k$ and $-\hat{s}_k$ will be decoded to the same bits. The transmitter does not need to send any side information. The receiver can make decisions of the transmitted symbols independently. The decoding errors of one subchannel does not affect other subchannels at all. The smallest PAPR using the SPR method can be found by exhausting all possible

combinations of rotations for the PR subchannel. We will show that when the subchannels are chosen properly, the optimal rotations of the PR subchannels can be computed efficiently. As the optimal solution is found by an exhaustive search (ES), we will call it SPR-ES. To further reduce the complexity, we propose an iterative approach (SPR-IT) to find suboptimal rotating for the PR subchannels. There is around 10 reduction in complexity. We will see that our method provides a tradeoff before PAPR reduction and complexity.

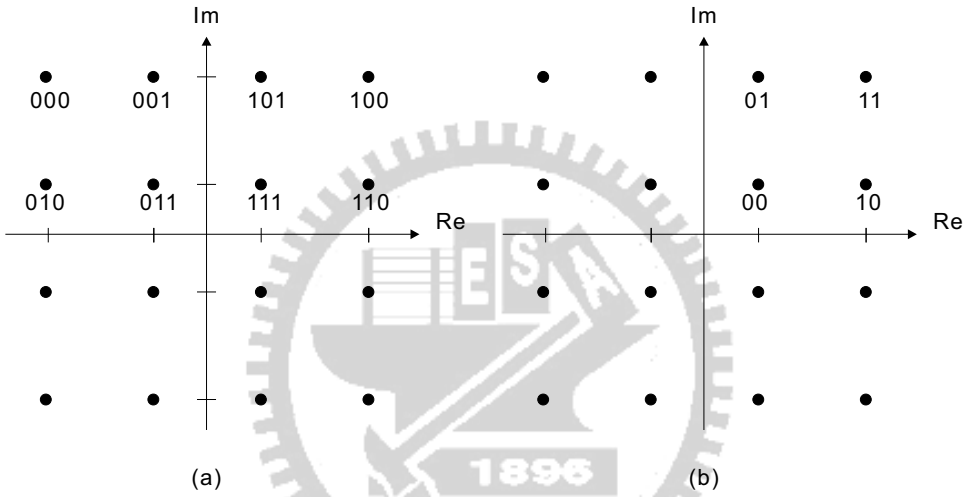

Figure 4.1: An example of bits-to-symbol mapping for PR subchannel when the constellation is 16 QAM. (a) The symbols on the PR subchannels may be rotated by multiples of 180°. (b) The symbol can be rotated by multiples of 90°.

4.1 An Exhaustive Search Scheme

Fig. 4.2 shows the block diagram of the SPR method. In the stage of initial bit-to-symbol mapping, the input bits are mapped to symbols. For non PR subchannels, the bits are mapped to symbols in the usual manner. For PR subchannels (180°-rotation case), the bits are mapped to symbols in the first and second quadrants as demonstrated in the example show in Fig. 4.1(a). The output vector of bits-to-symbol mapping is $\mathbf{s}$ as indicated in Fig. 4.2. We can write it as the sum of two vectors, one containing only non PR subchannels and the other containing

only PR subchannels,

$$\mathbf{s} = \mathbf{s}_0 + \mathbf{s}_1. \tag{4.1}$$

Suppose the PR subchannels are those with indices equal to multiples of J, then

$$\mathbf{s}_0 = \begin{bmatrix} 0 \\ s_1 \\ \vdots \\ s_{J-1} \\ 0 \\ s_{J+1} \\ \vdots \\ s_{2J-1} \\ 0 \\ \vdots \end{bmatrix}, \mathbf{s}_1 = \begin{bmatrix} s_0 \\ 0 \\ \vdots \\ 0 \\ s_J \\ 0 \\ \vdots \\ 0 \\ s_{2J} \\ \vdots \end{bmatrix}.$$

These two vectors are respectively the output of ′non PR vector′ and ′PR subchannel vector′ shown in Fig. 4.2.

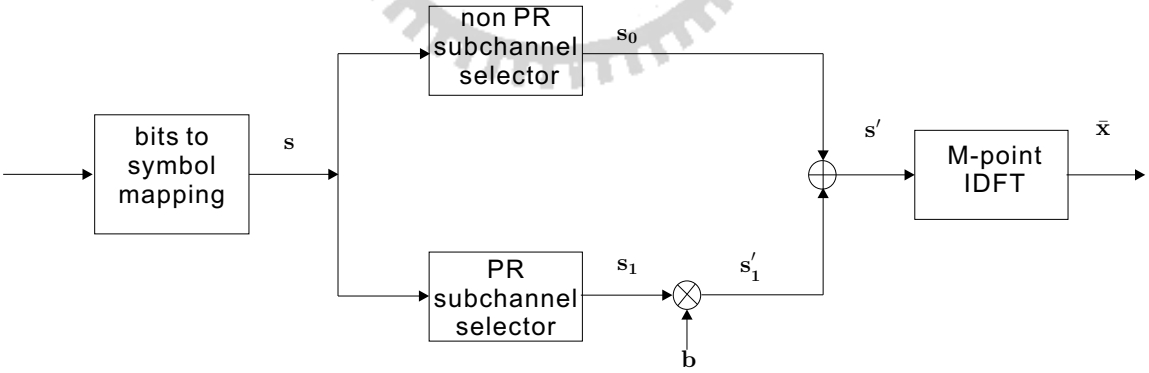

Figure 4.2: The block diagram of SPR method

We can generate all possible combinations of rotations of the PR subchannels. $\mathbf{s}'_1 = \mathbf{b} \,.\times \mathbf{s}_1$, where $\mathbf{b}$ is an $M \times 1$ vector with

$$[\mathbf{b}]_k = \begin{cases} 1 \quad \text{or} \quad -1, & \text{k=m}J \\ 0, & \text{otherwise.} \end{cases} \tag{4.2}$$

The notation $.\times$ denotes pointwise multiplication. The input vector of IDFT matrix is

$$\mathbf{s}' = \mathbf{s}_0 + \mathbf{s}'_1. \tag{4.3}$$

The output vector of the IDFT matrix is $\bar{\mathbf{x}} = \mathbf{w}^{\dagger}\mathbf{s}'$. For each possible rotation of the PR subchannels, we can compute the output vector and the PAPR of the output vector. We can then select the vector with the smallest PAPR.

We can also extend the method to the case of 90° rotations. In this case, the symbols of the PR subchannels may be rotated by multiples of 90°. The bit-to-symbol mapping is like Fig. 4.1(b). Also the $M \times 1$ rotation vector $\mathbf{b}$ can be written as

$$[\mathbf{b}]_k = \begin{cases} 1 \quad \text{or} \quad -1 \quad \text{or} \quad \text{j} \quad \text{or} \quad -\text{j}, & \text{k=m}J \\ 0, & \text{otherwise.} \end{cases} \tag{4.4}$$

The other process is the same. We defined $n = 2$ and $n = 4$ for multiplies of 180° and 90°.

In the following two examples, the IDFT size is 64 and 16 QAM with minimum distance $d = 2$ are used. A total 10^6 random OFDM blocks are used in simulation. We consider three different numbers of PR subchannels $P = 2$, 4, and 8 for the low complexity purpose which will discuss in chapter 5. We choose $n = 2$.

Example 4.1. We selected the 0-th and 31−th subchannel. For $P = 4$, the PR subchannels are 0-th, 15−th, 31-th, and 47-th subchannel. The 8 PR subchannels are 0-th, 7-th, 15-th, 23-th, 31-th, 39-th, 47-th, and 56-th subchannel. Fig. 4.3 shows the CCDF of PAPR for the case 180° rotation is used (n=2). The definition of CCDF for PAPR is as given in (2.5). For a CCDF of 10^{-4}, We can see the 2 PR subchannels curve reduces about 0.5dB compares with the original OFDM transmitter and the PAPR reduction are almost 1dB and 2dB for 4 PR subchannels and 8 PR subchannels curves respectively.

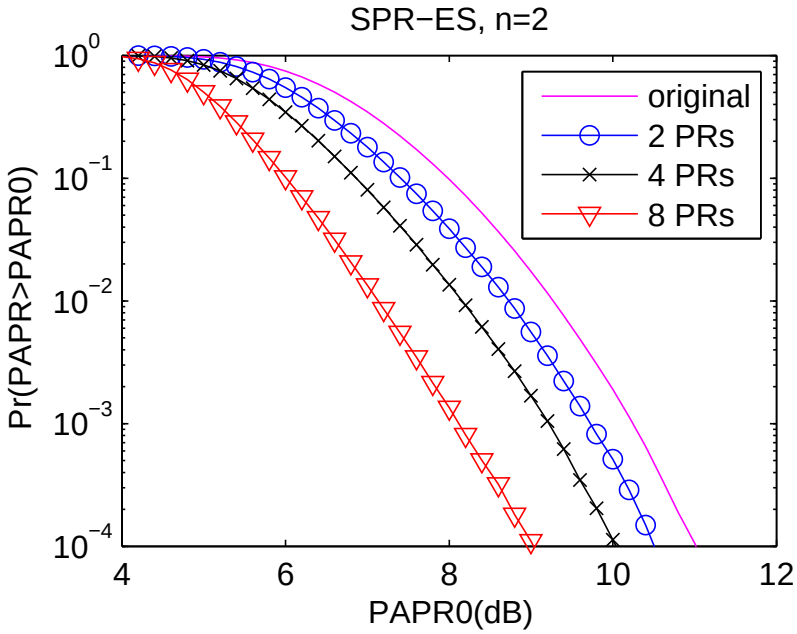

Figure 4.3: **Example 4.1**. SPR-ES: 2, 4, 8 PR subchannels and rotation factors are selected from $\{+1, -1\}$.

Example 4.2. In this example, we select the rotation factors from $\{+1, -1, +j, -j\}$. The numbers of PR subchannels of ES are 2 and 4 and the corresponding selected PR subchannels are $\{0, 31\}$ and $\{0, 15, 31, 47\}$. From Fig. 4.4, when CCDF is 10^{-4}, the 2 PR subchannels curve reduces about 0.7dB. The performance of 4 PR subchannels is 1.2dB better than the original OFDM system.

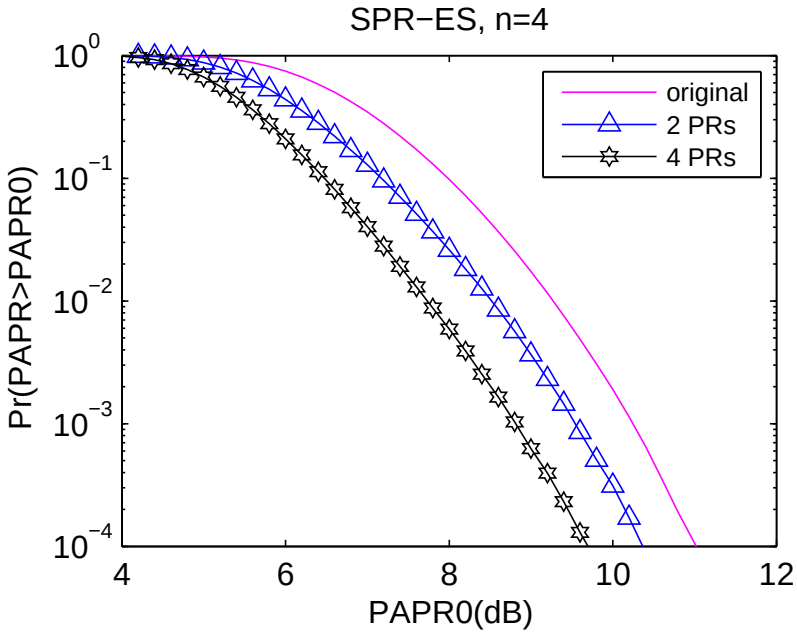

Figure 4.4: **Example 4.2**. SPR-ES: 2, 4 PR subchannels and rotation factors are selected from $\{+1, -1, +j, -j\}$.

4.2 An Iterative Approach Method

In the exhaustive method, we exhaust all possible combinations of rotations on the PR subchannels and choose the one that results in the smallest PAPR. Here we find the rotations for the PR subchannels in an iterative manner, one subchannel at a time.

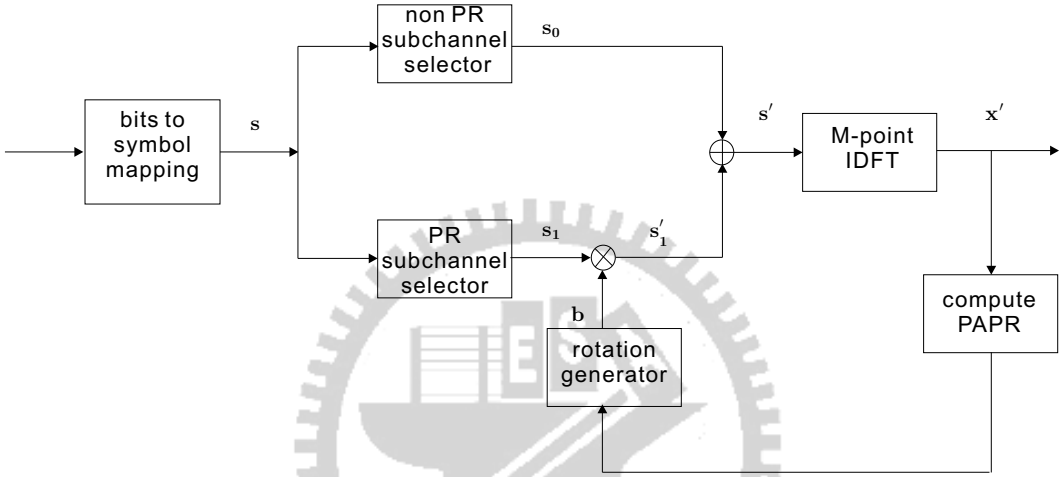

Figure 4.5: The block diagram of Iterative Approach method.

The block diagram is shown in Fig. 4.5. The input bits are mapped to symbols in the initial mapping as in the exhaustive method. Then we compute the IDFT output $\mathbf{x} = \mathbf{W}^\dagger \mathbf{s}$ and the corresponding PAPR. We find the peak on the IDFT output vector $\mathbf{x}$. Say the peak occurs at n_0 and $|x_{n_0}| = \max_i |x_i|$. Suppose now we would like to see if the rotation of a PR subchannel, say i_0, can reduce the peak. We split the subchannels into $\mathbf{s}_0$ and $\mathbf{s}_1$. The vector $\mathbf{s}_1$ is non zero only in the i_0th entry, $\mathbf{s}_1 = [0 \cdots 0 s_{i_0} 0 \cdots 0]^T$. When the i_0-th subchannel is rotated by 180°, we have $\mathbf{s}'_1 = -\mathbf{s}_1$. The new IDFT output $\mathbf{x}'$ can also be written as

$$\begin{aligned} \mathbf{x}' &= \mathbf{W}^\dagger(\mathbf{s}_0 + \mathbf{s}'_1) && (4.5) \\ &= \mathbf{W}^\dagger(\mathbf{s}_0 + \mathbf{s}_1 - 2\mathbf{s}_1) && (4.6) \\ &= \mathbf{W}^\dagger \mathbf{s} - 2\mathbf{W}^\dagger \mathbf{s}_1 && (4.7) \end{aligned}$$

Notice that $\mathbf{W}^\dagger \mathbf{s}$ is the original IDFT output $\mathbf{x}$ and $\mathbf{s}_1$ has only one nonzero entry

s_{i_0}, so we have

$$\mathbf{x}' = \mathbf{x} - 2\mathbf{w}_{i_0}^* s_{i_0}, \tag{4.8}$$

where $\mathbf{w}_{i_0}^*$ is the i_0-th column of the DFT matrix and '$*$' denotes conjugate. (4.8) means that $\mathbf{x}'$ can be obtained by computing $2\mathbf{w}_{i_0}^* s_{i_0}$ and subtracting it from $\mathbf{x}$. The computation of $2\mathbf{w}_{i_0}^* s_{i_0}$ requires only M multiplications and no addition.

We compute only the samples corresponding to the peak and find the new peak for $\mathbf{x}'$. If it is smaller than the peak of x_{n_0} then the i_0th subchannel is rotated by 180°. Otherwise, it is not rotated. In a similar manner, we can determine one by one the transmitted symbols on the PR subchannels. As the rotations on the PR subchannels are not determind simultaneously, the solution is the suboptimal one.

In the following two examples, the IDFT size is 64 and modulation symbols are 16 QAM with minimum distance $d = 2$. Total 10^6 random OFDM blocks are used.

Example 4.3. IT method is used. The number of PR subchannels are 2, 4, and 8 and the subchannels are chosen as : $\{0, 31\}$, $\{0, 15, 31, 47\}$, and $\{0, 7, 15, 23, 31, 39, 47, 56\}$. Fig. 4.6 show that case the symbols on SPR subchannels are possible rotated by 180° ($n = 2$). We can see that there is more reduction in PAPR as the number of 8.

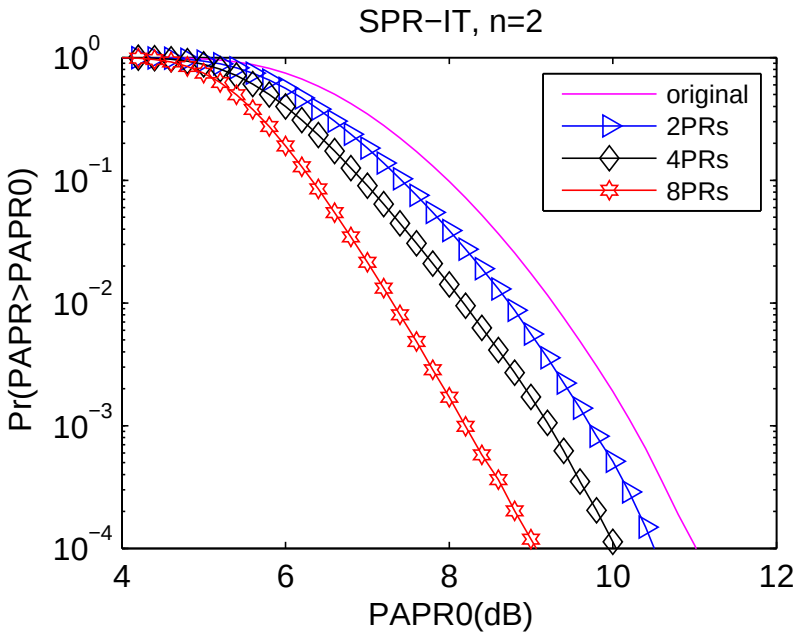

Figure 4.6: **Example 4.3**. SPR-IT: 2, 4, 8 PR subchannels and rotation factors are selected from $\{+1, -1\}$.

Example 4.4. Fig. 4.7 show that case of SPR-IT, the rotation factors set is $\{+1, -1, +j, -j\}$ and the PR subchannel selections: $\{0, 31\}$ for 2 PR subchannels, $\{0, 15, 31, 47\}$ for 4 PR subchannels, are the same as Fig. 4.4 for SPR-ES method. The two curves reduce at least 0.7 dB and 1.2dB of a CCDF 10^{-4} respectively. From Fig. 4.3 and Fig. 4.7, we find that when fixed the same set of rotation factors, the more PR subchannels we select and the more PAPR reduction at the same value of CCDF.

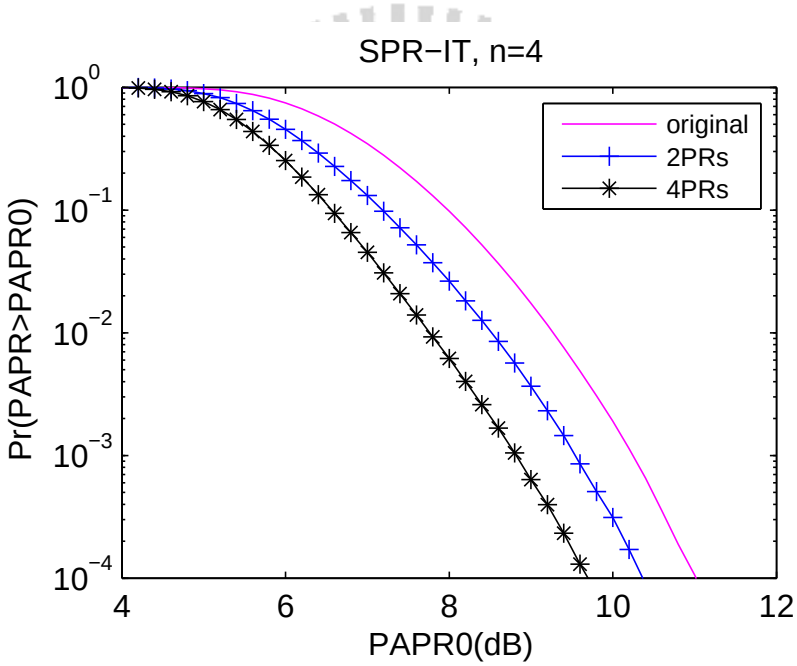

Figure 4.7: **Example 4.4**. SPR-IT: 2, 4 PR subchannels and rotation factors are selected from $\{+1, -1, +j, -j\}$.

Example 4.5. In Fig. 4.8, we put two methods together with the same number of PR subchannels, which are $\{0, 7, 15, 23, 31, 39, 47, 56\}$ and the same rotation factors set: $\{+1, -1\}$. As we mentioned in Chapter 2, for a given PAPR_0, the smaller the probability exceeds the PAPR_0 is, the better the performance is. We can see that exhaustive has better performance than iterative, especially when the PAPR thresholds are small. When the PAPR threshold PAPR_0 is 6dB, the probability exceeds PAPR_0 are 0.3 and 0.1 for SPR-IT and SPR-ES method respectively.

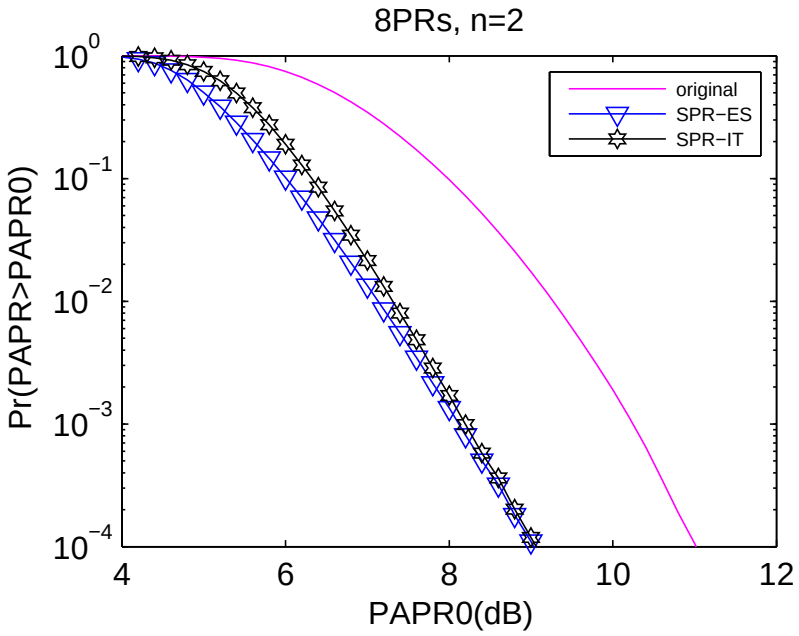

Figure 4.8: **Example 4.5**. SPR-ES v.s SPR-IT. 8 PR subchannels and rotation factors selected are from $\{+1, -1\}$.

Chapter 5

Computational Complexity

In this chapter, we consider the complexity of the SPR method proposed in chapter 4. We will also compare it with the tone injection method in chapter 3.

5.1 Exhaustive Search

The block diagram for the SPR method show in Fig. 4.2 can be drawn as Fig. 5.1. In Fig. 5.1, the IDFT block was put in front of the adder. We note that most of the elements only multiplies of J. As the result, the M-point IDFT after $\mathbf{s}_1^{'}$ in Fig. 5.1(a) can be replaced by a P-point IDFT. In Fig. 5.1(b), when P is defined as the number of PR subchannels. This can be done by using the lemma.

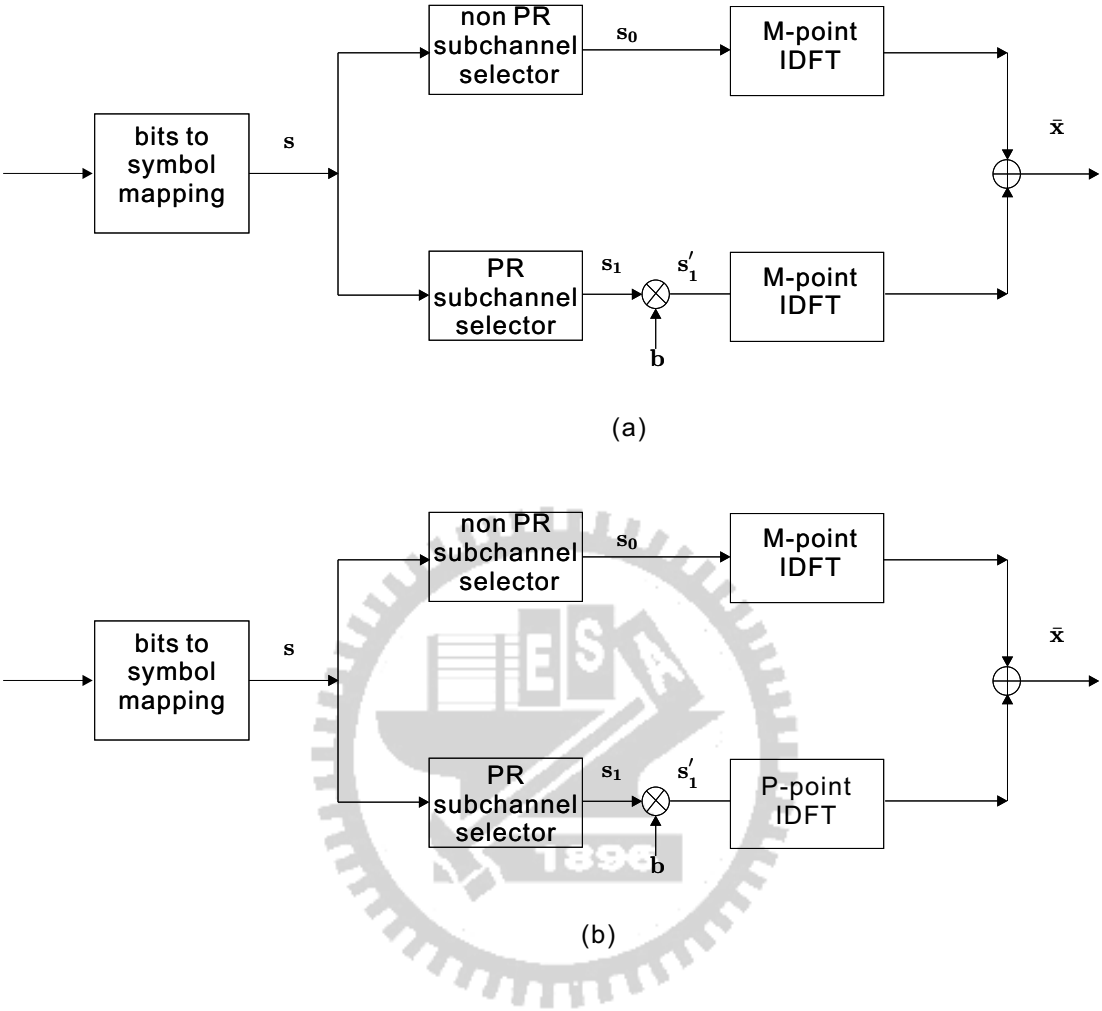

Figure 5.1: SPR-ES. (a) The IDFT block can put in front of the adder. (b) The M-point IDFT can be replaced by the P-point IDFT.

Lemma 1 *Let $\boldsymbol{W}_M^{\dagger}$ be the M-point IDFT matrix. Assume $M = J \times P$ for some integers J and P. Define a $P \times 1$ vector $\boldsymbol{z}' = [z_0, z_J, \cdots, z_{(P-1)J}]^T$. Define a $M \times 1$ vector $\boldsymbol{z}$, where*

$$[\boldsymbol{z}]_k = \begin{cases} z_k, & k{=}mJ, \quad m = 0, 1, \cdots, P-1 \\ 0, & \textit{otherwise.} \end{cases} \tag{5.1}$$

Then we have

$$\boldsymbol{W}_M^{\dagger}\boldsymbol{z} = \frac{1}{\sqrt{J}} \begin{bmatrix} \boldsymbol{W}_P^{\dagger} \\ \boldsymbol{W}_P^{\dagger} \\ \vdots \\ \boldsymbol{W}_P^{\dagger} \end{bmatrix} \boldsymbol{z}'.$$

Proof: Let $\mathbf{a} = \mathbf{W}_M^{\dagger}\mathbf{z}, \quad 0 \le n \le M-1$, then

$$a_n = \frac{1}{\sqrt{M}} \sum_{k=1}^{M-1} z_k e^{j2\pi kn/M} \tag{5.2}$$

$$= \frac{1}{\sqrt{M}} (z_0 e^{j2\pi n0/M} + z_J e^{j2\pi nJ/M} + \cdots + z_{(P-1)J} e^{j2\pi n(P-1)J/M}). \tag{5.3}$$

Let $\mathbf{g} = \frac{1}{\sqrt{J}}\mathbf{W}_P^{\dagger}\mathbf{z}', \quad 0 \le n \le P-1$, then

$$g_n = \frac{1}{\sqrt{J}} \frac{1}{\sqrt{P}} \sum_{k=1}^{P-1} z_k e^{j2\pi kn/P} \tag{5.4}$$

$$= \frac{1}{\sqrt{J}} \frac{1}{\sqrt{P}} (z_0 e^{j2\pi n0/P} + z_J e^{j2\pi n1/P} + \cdots + z_{(P-1)J} e^{j2\pi n(P-1)/P}). \tag{5.5}$$

Firstly, we proof that the first P elements of $\mathbf{a}$ are equal to $\mathbf{g}$, i.e., $a_l = g_l$ for $0 \le l \le P-1$. The l-th element of $\mathbf{a}$ is given by

$$a_l = \frac{1}{\sqrt{M}} (z_0 e^{j2\pi l0/M} + z_J e^{j2\pi lJ/M} + \cdots + z_{(P-1)J} e^{j2\pi l(P-1)J/M}) \tag{5.6}$$

$$= \frac{1}{\sqrt{J}} \frac{1}{\sqrt{P}} (z_0 e^{j2\pi l0/P} + z_J e^{j2\pi l/P} + \cdots + z_{(P-1)J} e^{j2\pi l(P-1)/P}) \tag{5.7}$$

$$= g_l, \quad for \quad 0 \le l \le P-1. \tag{5.8}$$

Secondly, we will show the following elements of $\mathbf{a}$ will repeat a_0 to a_{P-1}, i.e., $a_{l+q\cdot P} = a_l$, $0 \le l \le P-1$, $q = 1, \cdots, J-1$. The $(l + q \cdot P)$-th element of $\mathbf{a}$ is

given by

$$\begin{aligned} a_{l+q\cdot P} &= \tfrac{1}{\sqrt{M}}(z_0 e^{j2\pi(l+q\cdot P)0/M} + z_J e^{j2\pi(l+q\cdot P)J/M} + \cdots \\ &+ z_{(P-1)J} e^{j2\pi(l+q\cdot P)(P-1)J/M}) \\ &= \tfrac{1}{\sqrt{M}}(z_0 e^{j2\pi l0/M} e^{j2\pi q\cdot P0/M} + z_J e^{j2\pi lJ/M} e^{j2\pi q\cdot PJ/M} + \cdots \\ &+ z_{(P-1)J} e^{j2\pi l(P-1)J/M} e^{j2\pi q\cdot P(P-1)J/M}) \\ &= \tfrac{1}{\sqrt{M}}(z_0 e^{j2\pi l0/M} + z_J e^{j2\pi lJ/M} + \cdots + z_{(P-1)J} e^{j2\pi l(P-1)J/M}) \\ &= a_l \end{aligned} \tag{5.9}$$

We can see the first P elements of $\mathbf{a}$ are equal to $\mathbf{g}$ and the next every P elements of $\mathbf{a}$ repeated the first P elements of $\mathbf{a}$. △△△

From the proof we can see that the elements of $\mathbf{W}_M^\dagger \mathbf{z}$ can be viewed as the elements of $\frac{1}{\sqrt{J}}\mathbf{W}_P^\dagger \mathbf{z}'$ repeating J times.

The output vector $\bar{\mathbf{x}}$ can be written as

$$\begin{aligned} \bar{\mathbf{x}} &= \mathbf{W}^\dagger \mathbf{s}^{'} && (5.10)\\ &= \mathbf{W}^\dagger(\mathbf{s}_0 + \mathbf{s}_1^{'}) && (5.11)\\ &= \mathbf{W}^\dagger \mathbf{s}_0 + \mathbf{W}^\dagger \mathbf{s}_1^{'} && (5.12)\\ &= \mathbf{W}^\dagger \mathbf{s}_0 + \mathbf{W}^\dagger(\mathbf{b}\,.\times \mathbf{s}_1) && (5.13)\\ &= \mathbf{x} - \mathbf{W}^\dagger \mathbf{s}_1 + \mathbf{W}^\dagger(\mathbf{b}\,.\times \mathbf{s}_1). && (5.14) \end{aligned}$$

Let us look into the last term of (5.13). When a rotation vector $\mathbf{b}_i = u\mathbf{b}_k$, where $i, k \in \{0, 1, \cdots, n^P - 1\}$, and $u \in \{-1, +j, -j\}$, then

$$\begin{aligned} \mathbf{W}^\dagger(\mathbf{b}_i\,.\times \mathbf{s}_1) &= \mathbf{W}^\dagger(u\mathbf{b}_k\,.\times \mathbf{s}_1) && (5.15)\\ &= u\mathbf{W}^\dagger(\mathbf{b}_k\,.\times \mathbf{s}_1). && (5.16) \end{aligned}$$

Because multiplying u does not need any complex multiplication and complex addition, the complexity will not increase. For $n = 2$, by using (5.16) to get the values of $-\mathbf{W}^\dagger(\mathbf{b}_i\,.\times \mathbf{s}_1)$ and $\mathbf{W}^\dagger(\mathbf{b}_i\,.\times \mathbf{s}_1)$ we only need to calculate $\mathbf{W}^\dagger(\mathbf{b}_i\,.\times \mathbf{s}_1)$. It is the same as $n = 4$. Also we can apply lemma 1, then the M-point IDFT

can be replaced by a P-point IDFT. There are n^P possible $\mathbf{b}_i$. In conclusion, we only need $\frac{n^P}{n}$ P-point IDFTs instead of n^P P-point IDFTs to compute the optimal rotations for the smallest PAPR. For a IDFT matrix size M which is the power of 2, we can apply a fast algorithm-Inverse Fast Fourier Transform (IFFT). The number of complex multiplications and complex additions required for an M-point IFFT are $\frac{1}{2}M\log_2 M$ and $M\log_2 M$.

5.2 Iterative Approach

The iterative approach requires less complexity than the exhaustive method. Let us first consider one iteration. Recall from (4.5) when the i_0-th subchannel is rotated , the computation of the new DFT $\mathbf{x}^{'}$ is

$$\mathbf{x}^{'} = \mathbf{W}^{\dagger}\mathbf{s}^{'} = \mathbf{W}^{\dagger}(\mathbf{s}_0 + \mathbf{s}_1^{'}) \tag{5.17}$$

The vector $\mathbf{s}_1^{'} = r\mathbf{s}_1$ and $\mathbf{s}_1 = [0\cdots 0 s_{i_0} 0\cdots 0]^T$, where r is the rotation factor and i_0 is the underlying PR subchannel. When 180° rotation used $r = -1$, when 90° is used, $r = -1, \pm j$. We note that the term $\mathbf{x}_1^{'} = \mathbf{W}^{\dagger}\mathbf{s}_1^{'}$ can be written as $\mathbf{x}^{'} = r\mathbf{W}^{\dagger}\mathbf{s} = rs_{i_0}\mathbf{w}_{i_0}^{*}$, where $\mathbf{w}_{i_0}$ is the i_0-th column of DFT matrix and $'*'$ denotes conjugate. The computation of $\mathbf{x}^{'}$ needs only complex multiplications, but it does not need IDFT.

For the 180°-rotaion case ($n = 2$), when the i_0-th subchannel is rotated by 180°, the output vector $\mathbf{x}^{'} = \mathbf{x} - 2s_{i_0}\mathbf{w}_{i_0}^{*}$. To compute $\mathbf{x}^{'}$, we need M complex multiplications and M complex additions. If we have P PR subchannels, the total complexity is PM complex multiplications and additions.

For the 90°-rotation case ($n = 4$), $r = -1, \pm j$. The output $\mathbf{x}^{'}$ can be written as

$$\begin{aligned}
\mathbf{x}^{'} &= \mathbf{W}^{\dagger}\mathbf{s}_0 + \mathbf{W}^{\dagger}\mathbf{s}_1^{'} && (5.18)\\
&= \mathbf{W}^{\dagger}\mathbf{s}_0 + \mathbf{W}^{\dagger}(r_i\mathbf{s}_1^{'}) && (5.19)\\
&= \mathbf{x} - \mathbf{W}^{\dagger}\mathbf{s}_1 + rs_{i_0}\mathbf{w}_{i_0}^{*}. && (5.20)\\
&= \mathbf{x} - s_{i_0}\mathbf{w}_{i_0}^{*} + rs_{i_0}\mathbf{w}_{i_0}^{*}. && (5.21)
\end{aligned}$$

If $r_i = -1$, we need M complex multiplications and additions. For $r_i = j$ or $-j$, no complex multiplication is needed but $3M$ complex additions are needed for computing $\mathbf{x} - s_{i_0}\mathbf{w}_{i_0}^*$, $+js_{i_0}\mathbf{w}_{i_0}^*$, and $-js_{i_0}\mathbf{w}_{i_0}^*$. A total of MP complex multiplications and $4MP$ complex additions are needed for P PR subchannels in SPR-IT method.

If the PR subchannel is selected properly, computing $s_{i_0}\mathbf{w}_{i_0}^*$ does not need any complex multiplication. For example, when $M = 64$, the 0-th subchannel is selected to be the PR subchannel.

$$s_0\mathbf{w}_0^* = s_0 \begin{bmatrix} 1 \\ 1 \\ \vdots \\ 1 \end{bmatrix}. \tag{5.22}$$

No complex multiplication is needed to compute (5.22).

5.3 Tone Injection (for passband communication)

Tone injection proposed by J. Tellado [6] is in the consideration of real multicarrier. We modified it to passband communication in section 3.2 and in this section we will calculate the complexity. We will divided $\mathbf{s}$ into two vectors like SPR method. One is a $M \times 1$ vector $\mathbf{s}_1$ contained one subchannel which is going to be modified, the other is a $M \times 1$ vector $\mathbf{s}_0 = \mathbf{s} - \mathbf{s}_1$. Suppose the k-th subchannel is going to change. We can write down $\mathbf{s}_1$ which has only one value on the k-th subchannel,

$$\mathbf{s}_1 = \begin{bmatrix} 0 \\ \vdots \\ 0 \\ s_k \\ 0 \\ \vdots \\ 0 \end{bmatrix}.$$

Subtract $\mathbf{s}$ by $\mathbf{s}_1$ then we get a vector $\mathbf{s}_0$,

$$\mathbf{s}_0 = \begin{bmatrix} s_0 \\ s_1 \\ \vdots \\ s_{k-1} \\ 0 \\ s_{k+1} \\ \vdots \\ s_{M-1} \end{bmatrix}.$$

After modification which was discussed in section 3.2, $\mathbf{s}_1$ becomes $\bar{\mathbf{s}}_1$:

$$\bar{\mathbf{s}}_1 = \begin{bmatrix} 0 \\ \vdots \\ 0 \\ s_k \\ 0 \\ \vdots \\ 0 \end{bmatrix} + p_k D \begin{bmatrix} 0 \\ \vdots \\ 0 \\ 1 \\ 0 \\ \vdots \\ 0 \end{bmatrix} + jq_k D \begin{bmatrix} 0 \\ \vdots \\ 0 \\ 1 \\ 0 \\ \vdots \\ 0 \end{bmatrix} \tag{5.23}$$

$$= \mathbf{s}_1 + (p_k D + jq_k D)\mathbf{e}_k, \tag{5.24}$$

where $\mathbf{e}_k = [0, \cdots, 0, 1, 0, \cdots, 0]^T$. Let $m = p_k D + jq_k D$. After IDFT matrix, we get

$$\bar{\mathbf{x}} = \mathbf{W}^\dagger(\mathbf{s}_0 + \bar{\mathbf{s}}_1) \tag{5.25}$$

$$= \mathbf{W}^\dagger \mathbf{s}_0 + \mathbf{W}^\dagger \bar{\mathbf{s}}_1 \tag{5.26}$$

(5.26) can also be written as

$$\bar{\mathbf{x}} = \mathbf{x} - \mathbf{W}^\dagger \mathbf{s}_1 + \mathbf{W}^\dagger \bar{\mathbf{s}}_1 \tag{5.27}$$

$$= \mathbf{x} - \mathbf{W}^\dagger \mathbf{s}_1 + \mathbf{W}^\dagger(\mathbf{s}_1 + m\mathbf{e}_k) \tag{5.28}$$

$$= \mathbf{x} + m\mathbf{W}^\dagger \mathbf{e}_k. \tag{5.29}$$

$\mathbf{W}^\dagger \mathbf{e}_k$ is equal to $1 \cdot \mathbf{w}_k^*$ and it does not need any IDFT matrix. For the k-th subchannel, m can be 9 different values because $p_k, q_k \in \{0, +1, -1\}$. We can classify m into three groups as below.

(i) When $m = 0$, $\bar{\mathbf{x}} = \mathbf{x}$. The M-point IDFT is not included in complexity calculation.

(ii) When $m = D$ or $m = jD$ or $m = -jD$ or $m = -D$. We need M complex multiplications for $m = D$ to multiply $\mathbf{w}_k^*$. $4M$ complex additions are also needed because here we have 4 values of m and each m needs M complex additions in (5.29).

(iii) The remainders: $m = D + jD$, $m = D - jD$, $m = -D + jD$, and $m = -D - jD$. When $m = D + jD$,

$$m\mathbf{W}^\dagger \mathbf{e}_k = (D + jD)\mathbf{W}^\dagger \mathbf{e}_k \tag{5.30}$$

$$= D\mathbf{W}^\dagger \mathbf{e}_k + jD\mathbf{W}^\dagger \mathbf{e}_k. \tag{5.31}$$

Both $D\mathbf{W}^\dagger \mathbf{e}_k$ and $jD\mathbf{W}^\dagger \mathbf{e}_k$ are calculated in (ii). Therefore, we do not need any complex multiplication but M complex additions to add $D\mathbf{W}^\dagger \mathbf{e}_k$ and $jD\mathbf{W}^\dagger \mathbf{e}_k$ together. $4M$ complex additions are the same purpose as in (ii). Then in this part we use only $5M$ complex additions and no complex multiplication.

Put three groups together then we realize that to change a subchannel use tone injection method needs M complex multiplications and $9M$ complex additions. For total M subchannels, the complexity becomes $M \times M$ complex multiplications and $9M \times M$ complex additions. When M gets larger, the complexity increase faster.

We put three methods comparison together in the following table.

Table 5.1: Complexity Comparison of the SPR-ES, SPR-IT, and Tone Injection methods. If $P \in \{0, \frac{M}{4} - 1, \frac{M}{2} - 1, \frac{3M}{4} - 1\}$, the complex multiplication of SPR-IT (n=2) and SPR-IT (n=4) are zero.

	complex multiplications	complex additions
SPR-ES	$\frac{1}{2}(n^{P-1})P\log_2 P$	$(n^{P-1})P\log_2 P + Mn^P$
SPR-IT ($n = 2$)	PM	PM
SPR-IT ($n = 4$)	PM	$4PM$
Tone Injection [6]	M^2	$9M^2$

Example 5.1 Both SPR-ES and SPR-IT select 8 PR subchannels: $\{0, 7, 15, 23, 31, 39, 47, 56\}$ and the rotation factors are selected from $\{+1, -1\}$. The IDFT size is 64. $a = 1$, $D = 8$ in Tone Injection method. The complexity comparison of the three methods are put in Table. 5.2

Table 5.2: **Example 5.1**. Complexity comparison of the SPR-ES, SPR-IT, and tone injection methods. 8 PR subchannels are selected for SPR-ES and SPR-IT and the rotation factors are selected from $\{+1, -1\}$. $a = 1$, $D = 8$ in tone injection method.

	complex multiplications	complex additions
SPR-ES	1536	19456
SPR-IT	256	1024
Tone Injection [6]	4096	36864

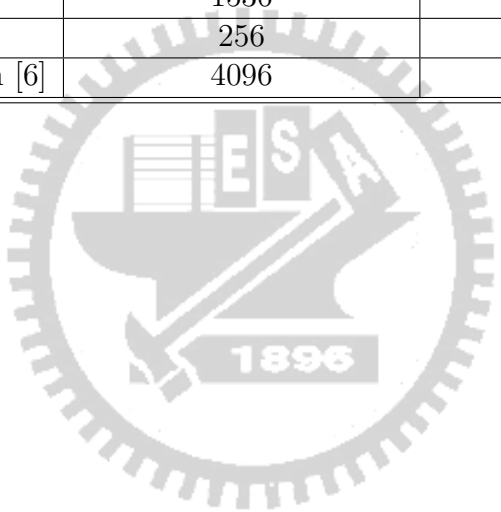

Chapter 6

Simulation Results

In this chapter we will see more simulation results. The block diagram of the OFDM system using SPR method is shown in Fig. 6.1. The IDFT block at the transmitter is put in the SPR method block in Fig. 4.2 and Fig. 4.5. The input symbols have the same variance ε_s because there is usually no bit/power allocation in the OFDM system. The symbols are assumed to be zero mean and uncorrelated, which is usually a reasonable assumption after proper interleaving of the input bit stream. The autocorrelation matrix of the input vector $\mathbf{s}$ is thus $\mathbf{R}_s = \varepsilon_s \mathbf{I}_M$, where $\mathbf{I}_M$ is a $M \times M$ identity matrix. Then the output vector of IDFT matrix $\mathbf{x} = \mathbf{W}^\dagger \mathbf{s}$ has autocorrelation matrix $\mathbf{R}_x = E[\mathbf{x}\mathbf{x}^\dagger]$ given by:

$$\mathbf{R}_x \;=\; \mathbf{W}^\dagger \mathbf{R}_s \mathbf{W} = \varepsilon_s \mathbf{I}_M. \tag{6.1}$$

Therefore $\mathbf{x}$ are uncorrelated and their variances are the same, equal to ε_s.

Fig. 6.2 shows the clipping with a maximum permissible amplitude A. The operation of clipping a real number x can be written as:

$$y = f(x) = \begin{cases} x, & |x| \le A \\ A, & |x| > A \end{cases} \tag{6.2}$$

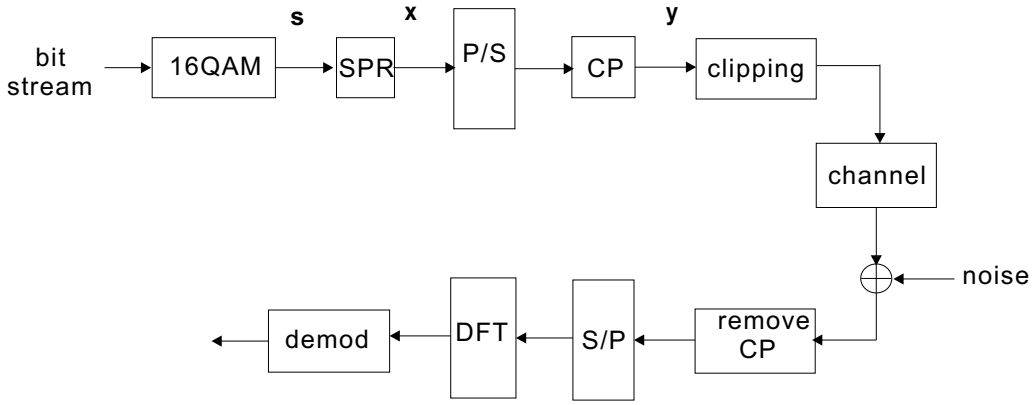

Figure 6.1: The OFDM system with SPR method.

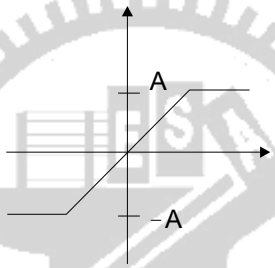

Figure 6.2: A clipping with maximum amplitude A.

In Fig. 6.1, there is a clipping block before the channel. The n-th element of the transmitted signal $\mathbf{y}$ can be written as

$$y_n = y_{r,n} + jy_{i,n}, \tag{6.3}$$

where $y_{r,n}$ and $y_{i,n}$ are the real and imaginary part of y_n respectively. The amplitude clipping operates on $y_{r,n}$ and $y_{i,n}$ individually. The output of clipper becomes $f(y_{r,n}) + jf(y_{i,n})$. The clipping ratio γ is defined as

$$\gamma = \frac{A_{\max}}{\sqrt{P_0}}, \tag{6.4}$$

where $A_{\max} = \sqrt{A^2 + A^2} = \sqrt{2}A$.

Here we use the commonly decision rule which called nearest neighbor decision rule (NNDR). For tone injection method, the decision regions of the two exterior

constellation points become smaller after modulo-D process and hence the bit error rate (BER) may be increased slightly.

The BER depends on the signal power and the noise power. The BER curves are plotted against the signal-to-noise (SNR). But here we will plot the BER curves of average-transmission-power-to-noise ratio (P_0/N_0), where P_0 is the average transmission power of $\mathbf{y}$ before clipping and N_0 be the noise variance of AWGN channel.

We will see some examples in the following. In our simulations, the IDFT size is 64 and total 10^5 random OFDM blocks are used in the simulation. The input symbols are 16 QAM. P_0 is the same as ε_s. The SPR method uses 8 PR subchannels: $\{0, 7, 15, 23, 31, 39, 47, 56\}$ and the rotation factors are selected from $\{+1, -1\}$. $a = 1$ in the tone injection method. We selected 8 PR subchannels and SPR-ES will lose 8 bits for a block transmission.

Fixed noise variance ($N_0 = 1$). The noise variance N_0 is fixed to 1. The BER of SPR-ES and tone injection are in Fig. 6.3. We can see under the same noise variance, SPR-ES has better BER performance. When BER is fixed to 10^{-3}, P_0 are 16.5 dB and 17.3 dB for SPR-ES and tone injection. This is meant that the average transmission power are 44.67 and 53.7 respectively. The average transmission power of SPR-ES is 20% smaller than tone injection. However, SPR-ES used 8 PR subchannels and lost 8 bits when 16 QAM constellation is used. This is equivalent to a loss of 3% in transmission rate. Under the same noise variance and BER, SPR-ES needs smaller average transmission power than tone injection. The CCDF of PAPR of both methods are in Fig. 6.4. For large PAPR0 SPR-ES has better performance than tone injection.

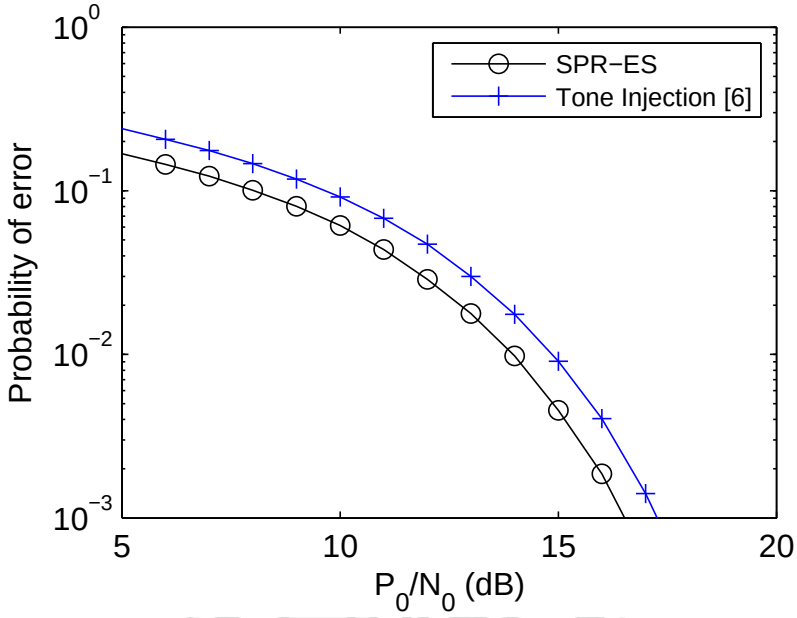

Figure 6.3: BER. N_0=1. SPR-ES uses 8 PR subchannels and rotation factors are selected from $\{+1, -1\}$ and tone injection.

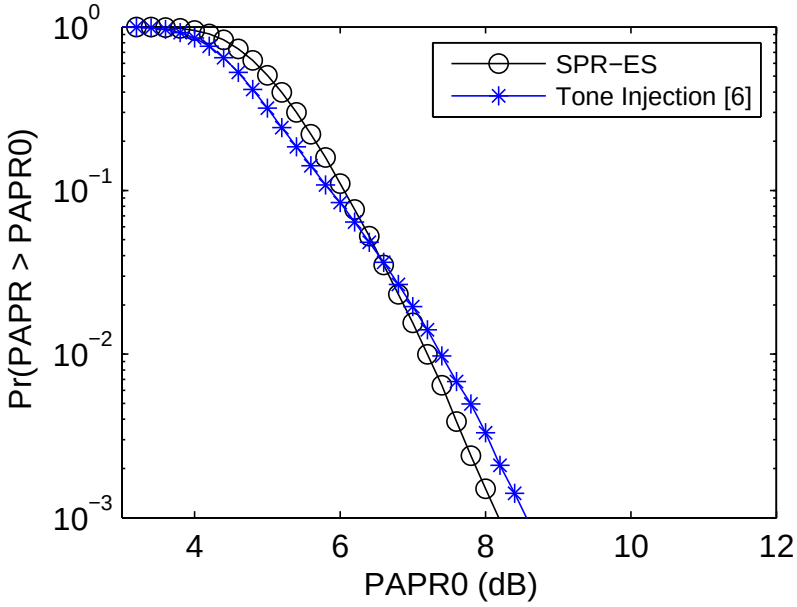

Figure 6.4: PAPR. N_0=1, BER=10^{-3}. SPR-ES uses 8 PR subchannels and rotation factors are selected from $\{+1, -1\}$ and tone injection.

Fixed average transmission power. ($P_0 = 10$). In this example, we fixed the average transmission power P_0 to 10. When fixed P_0, the minimum distance of the constellation used the tone injection method is smaller than that of SPR-ES. The minimum distance of SPR-ES and tone injection are 2 and 1.88 respectively. We can see SPR-ES has better BER performance in Fig. 6.5. For a BER of 10^{-3}, SPR-ES is 1 dB less than tone injection.

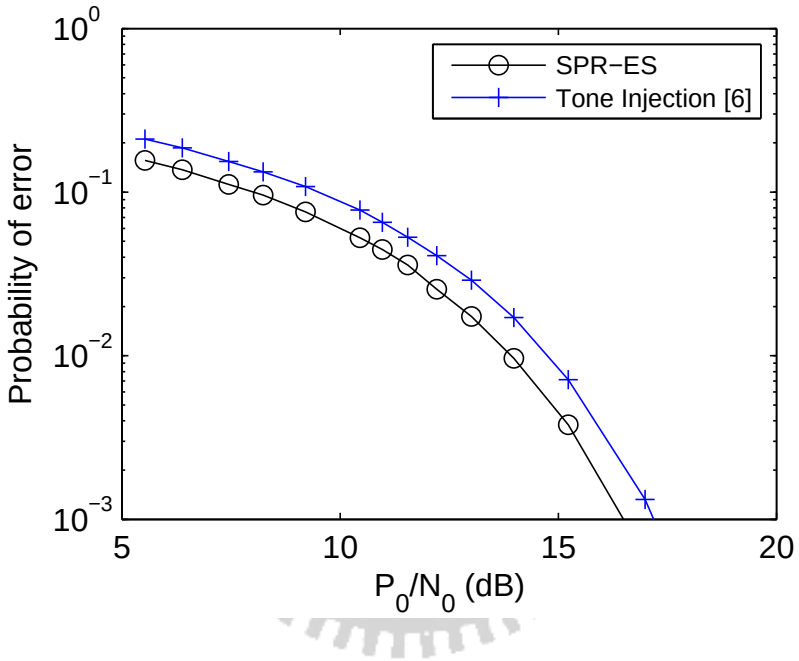

Figure 6.5: BER. **Fixed average transmission power.** $P_0 = 10$. SPR-ES uses 8 PR subchannels and rotation factors are selected from $\{+1, -1\}$ and tone injection.

Fixed average transmission power and the clipping ratio. ($P_0 = 10$, $\gamma = 2$). In the following two examples we add a clipping operator before the signal passing through the channel. The BER performance after adding the clipping is worse, especially for the smaller clipping ratio γ. If P_0 and γ are fixed, the peak value can be decided. When $\gamma = 2$ and $P_0 = 10$ we can get $A_{\max} = 6.32$ and the corresponding $A = 4.47$. The peak value of the two methods are all equal to $(4.47)^2 + (4.47)^2 = 39.96$. Under the same peak value and P_0, SPR-ES has slightly better BER performance.

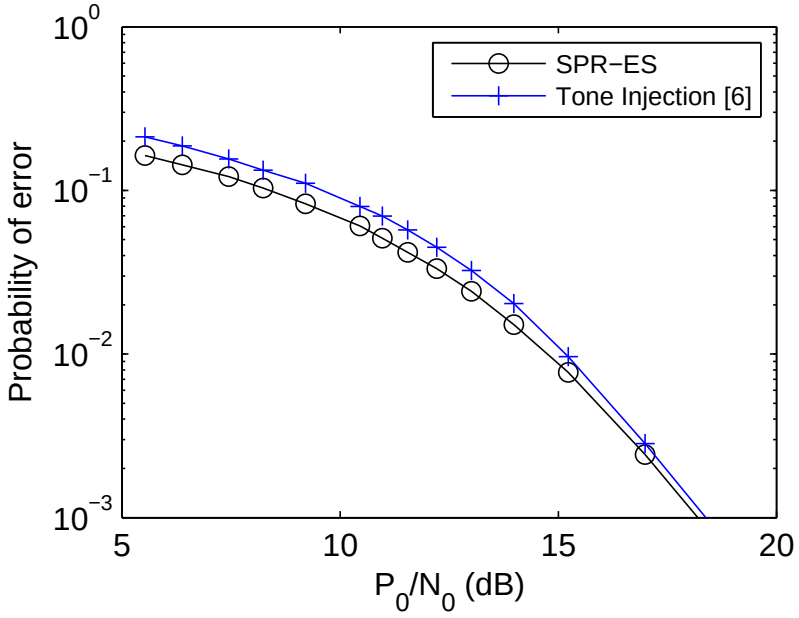

Figure 6.6: BER. **Fixed average transmission power and the clipping ratio.** ($P_0 = 10$, $\gamma = 2$). SPR-ES uses 8 PR subchannels and rotation factors are selected from $\{+1, -1\}$ and tone injection.

Fixed average transmission power and the clipping ratio. ($P_0 = 10$, $\gamma = 3$). In this example, $\gamma = 3$ and $P_0 = 10$. $A_{\max} = 9.49$ and the corresponding $A = 6.71$. The peak value of the two methods are all equal to $(6.71)^2 + (6.71)^2 = 90.05$. SPR-ES in this example still has better performance than the tone injection method.

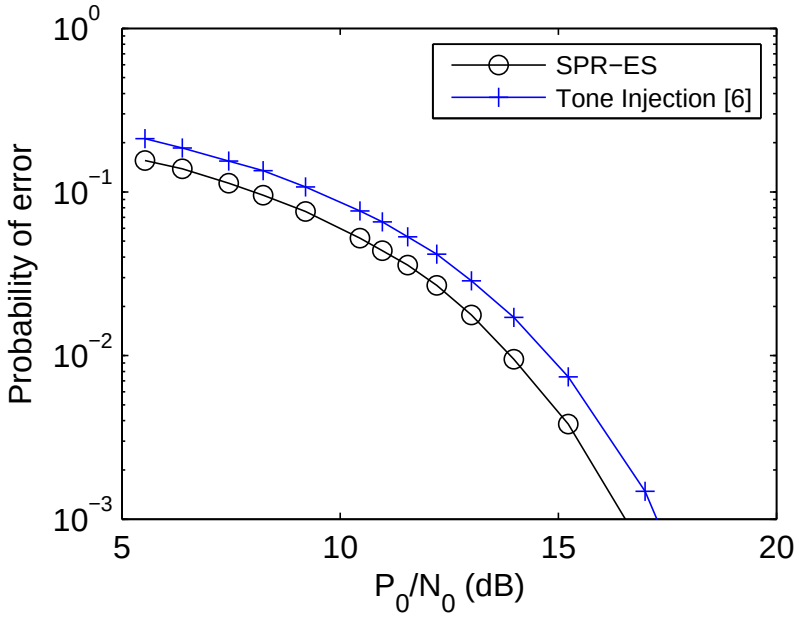

Figure 6.7: BER. **Fixed average transmission power and the clipping ratio.** ($P_0 = 10$, $\gamma = 3$). SPR-ES uses 8 PR subchannels and rotation factors are selected from $\{+1, -1\}$ and tone injection.

Chapter 7

Conclusion

In this thesis, we proposed a new method called SPR. SPR method reduces PAPR by multiplying rotations to the symbols of the PR subchannels individually. Two schemes of SPR method were introduced. Simulation results showed both shcemes can reduce at least half dB from the original system with no PAPR reduction method when only two PR subchannels were selected. The average transmission power of SPR method remains the same. A few bits were lost on the PR subchannels but no side information is needed. Although the computational complexity increases, the numbers of complex multiplications and complex additions are few compared with tone injection method.

Bibliography

[1] J. A. C. Bingham, "Multicarrier Modulation For Data Transmission: An Idea Whose Time Has Come," *IEEE Commun. Mag*, vol. 28, no. 5, May 1990, pp. 5-14.

[2] M. Aldinger, "Multicarrier COFDM scheme in high bit rate ratio local area network," in *Proc. 5th IEEE Int. Symp. Personal, Indoor and Mobile Radio Communications*, The Haugue, The Netherlands, Sept. 1994, pp. 969-973.

[3] ETSI, "Digital Video Broadcasting; Framing, Structure, Channel Coding and Modulation for Digital Terrestrial Television (DVB-T)," ETS 300 744, 1997.

[4] ETSI, "Digital Audio Broadcasting (DAB) to Mobile, Protable and Fixed Receivers," ETS 300 401, 1994.

[5] A. Ruiz, John M. Cioffi, and S. kasturia, Discrete Multiple Tone Modulation with Coset Coding for The Spectrally Shaped Channel, IEEE Transcation on Communications, Vol. 40, No. 6, Page (s) : 1012-1029, June 1992.

[6] J. Tellado, *Multicarrier Modulation with Low PAR: Applications to DSL and Wireless* Kluwer Acdamic, Press. 2000.

[7] R. O'Nell and L. B. Lopes, "Envelope Variations and Spectral Splatter in Clipped Multicarrier Signals," *Proc. IEEE PIMRC '95*, Toronto, Canada, Sept. 1995, pp. 71-75.

[8] A. E. Jones, T. A. Wilkinson, and S. K. Barton,"Block Coding Scheme for Reduction of Peak to Mean Envelope Power Ratio of Multicarrier Transmission Scheme," *Elect, Lett*, vol. 30, no. 22, Dec. 1994, pp. 2098-99.

[9] J. A. Davis, and J. Jedweb,"Peak-to-Mean Power Control in OFDM, Golay Complementary Sequences, and Reed-Muller Codes" *IEEE, Trans Info. Theory*, vol. 45, no. 7, Nov. 1999, pp. 2397-17.

[10] K. G. Paterson and V. Tarokh,"On the Existence and Construction of Good Codes with Low Peak-to-Average Power Ratios," *IEEE, Trans Info. Theory*, vol. 45, no. 6, Sept. 2002, pp. 1974-87.

[11] R. W. Bäuml, R. F. H. Fisher, and J. B. Huber, Reducting the Peak-to-Average Power Ratio of Multicarrier Modulation by Selected Mapping ," *Elect, Lett*, vol. 32, no. 22, Oct. 1996, pp. 2056-57.

[12] P. Van Eelvelt, G. Wade, and M. Tomlinson, Peak to average power reduction for OFDM schemes be selective scrambing.*Elect, Lett*,, vol. 32, no. 21, pp. 1963-1964, Oct. 1996.

[13] S. H. Müller and J. B. Huber, OFDM with Reduced Peak-to-Average Power Ratio by Optimum Combination of Partial Transmit Sequences,*Elect, Lett*, vol. 33, no. 5, Feb. 1997, pp. 368-69.

[14] C.-L. Wang, M.-Y. Hsu, and Y. Ouyang, A low-complexity peak-to-average power ratio reduction technique for OFDM systems, in Proc. 2003 IEEE Global Telecommun. Conf. (GLOBECOM 2003), San Francisco, CA, Dec. 2003, pp. 2375-2379.

[15] C.-L. Wang and Y. Ouyang,Low-Complexity Selected Mapping Schemes for Peak-to-Average Power Ratio Reduction in OFDM Systems, IEEE Transcation on Communications, Vol. 53, no. 12, Dec. 2005.

[16] S. H. Han and J. H. Lee, PAPR Reduction of OFDM Signals Using a Reduced Complexity PTS Technique, IEEE Sig. Proc. Lett., vol. 11, no. 11, Nov. 2004, pp. 887V90.